J. Fluid Mech. (1983), *vol.* 129, *pp.* 313–335
Printed in Great Britain

A theoretical model of absorption of gases by the bronchial wall

By M. R. DAVIDSON

Applied Mathematics and Computing Division, Australian Atomic Energy Commission Research Establishment, Lucas Heights Research Laboratories, Sutherland 2232, Australia

AND R. C. SCHROTER

Physiological Flow Studies Unit, Imperial College, London

(Received 24 March 1982 and in revised form 7 July 1982)

The pattern of dispersion and uptake of an inhaled slug of tissue-soluble gas is examined within a branching model of the bronchial airways of the human lung, considered as an assembly of segments from infinitely long, straight rigid tubes with absorbing walls of finite thickness. The model is based on the first three (time-dependent) spatial moments of the solute distribution in such tubes, determined by the Aris method of moments. Poiseuille flow in each airway is assumed, and the solute distribution is taken to be initially zero in the tissue and radially uniform in the gas. First, the time dependence of axial velocity and mixing coefficient of the advancing solute in infinitely long tubes is shown and the mechanisms responsible are discussed. Transit times, uptake, uptake efficiency and mixing coefficient predicted from the model are then shown for different flow rates and solubilities, as functions of the generation of branching. As is expected, greater penetration is found for lower-solubility gases. However, of greater interest is the model prediction that uptake decreases with increasing flow rate whereas uptake efficiency increases, a result consistent with experimental indications. Finally, the mixing coefficient is shown to fall, with distance into the lung, to a value which may be much smaller than the molecular diffusivity, depending on the solubility.

1. Introduction

The delicate alveolar membrane of the mammalian lung, at which respiratory gas exchange between the body and its surroundings takes place, requires protection from the environmental air. To achieve appropriate conditioning of the inspired air, it is heated to body temperature and humidified to saturation on its passage through the upper airway and bronchial airways of the lung. In addition, it is important to protect the alveolar membrane and blood from noxious substances in the atmosphere; these may be particulate or gaseous, either man-made or naturally occurring. Both the processes of humidification and removal of noxious gases involve mass transfer between the airstream and the walls of the respiratory tract. Although the deposition of particulate materials within the respiratory tract has received considerable attention both experimentally and theoretically, relatively little attention has been paid to the mechanisms of gas exchange between the upper airway or the bronchial walls and the respired air.

In recent years, experimental studies of gas uptake have focused strongly on two common atmospheric pollutants, sulphur dioxide and nitrogen dioxide (see e.g. Yokoyama 1968; Ichioka 1972). Yokoyama considered absorption in the isolated

upper airway of the dog and rabbit, whereas Ichioka constructed a highly simplified, non-branching physical model of the human bronchial tree from glass tubes lined with moistened filter paper. Both studies confirmed the greater penetration of the lower-solubility gas (NO_2). By changing the flow rate through his model, Ichioka showed that the uptake of NO_2 decreased as flow rate increased but that the uptake of SO_2 diminished only a little. Similar results may apply to other soluble gases.

Aharonson *et al.* (1974) conducted an interesting experimental and theoretical study of the uptake of a number of soluble gases (acetone, ether, O_3, SO_2) by the nasal passages of the dog. They showed that, although extraction certainly fell with increasing flow rate, the uptake efficiency (defined as the absorption rate per unit partial pressure in the gas stream) increased; they described their observations in terms of a simple one-dimensional model of the nose.

Miller, Menzel & Coffin (1978) simulated the dispersion and uptake of O_3 in the lung by numerically solving a bulk-averaged convection–diffusion equation with a source term to account for absorption in the bronchial wall. However, their prediction that ozone uptake increases with tidal volume which itself increases with flow rate (because of their choice of inspiration times) seems to contradict the experience of previous workers.

Since the majority of uptake studies have focused on the upper airway (i.e. the passages of the head and neck above the trachea), very little is known about events in the bronchial airways and alveoli. Uptake behaviour in the bronchial airways has simply been inferred from that in the upper airway, and consequently is in need of proper theoretical and experimental study. The purpose of this paper is to develop a theoretical model of the exchange of a certain class of soluble materials between the bronchial airway wall and the contained flowing gas under conditions which are appropriate to respiration in man. It is applied here to the initial inhalation of a gas mixture containing a slug of soluble material. Predicted uptake behaviour is compared with that observed experimentally, and the effect of uptake on the dispersion of gas along the bronchial tree is considered.

2. Geometry and structure of the bronchial airways

The tracheo-bronchial system which conducts gas to the alveoli of the lung is a tree-like branching structure whose main trunk (the trachea) starts below the larynx. The branching properties, although essentially dichotomous, generate a distinctly asymmetrical structure: thus although the average pathlength from trachea to terminal bronchiole is 13 cm in man, it can be as little as 8 cm (8 generations of branching) and as long as 22 cm (25 generations), as observed by Horsfield & Cumming (1968). Weibel (1963) developed a symmetrical equivalent model of the real system on the basis of extensive measurements of casts of human bronchial airways; the dimensions of the bronchi as reported by Weibel are used in the present study (see table 1). Individual bronchi are considered to be circular in cross-section, rigid and straight. The details of bronchial bifurcations and the complexities of flow patterns within the airways (Pedley, Schroter & Sudlow 1977) are ignored in this paper.

The microscopic structure of the bronchial wall is quite complex, but, for the purposes of wall gas exchange, the principal interest is in the structure between the mucosal surface and the layer of systemic capillaries lying closely underneath the epithelial lining of the wall, as shown schematically in figure 1. The liquid mucous lining covers a single layer of epithelial cells which in turn rest on a basement

Airway generation	Number of airways	Diameter (cm)	Total cross-section (cm^2)	Length (cm)	Wall thickness (cm)
0	1	1·8	2·54	12	0·09
3	8	0·56	2·00	0·76	0·028
6	64	0·28	3·96	0·90	0·014
10	1024	0·130	13·4	0·46	0·0065
16	65536	0·060	180·0	0·165	0·0030

TABLE 1. Selected bronchial airway and wall dimensions following Weibel (1963) and DuBois & Rogers (1968)

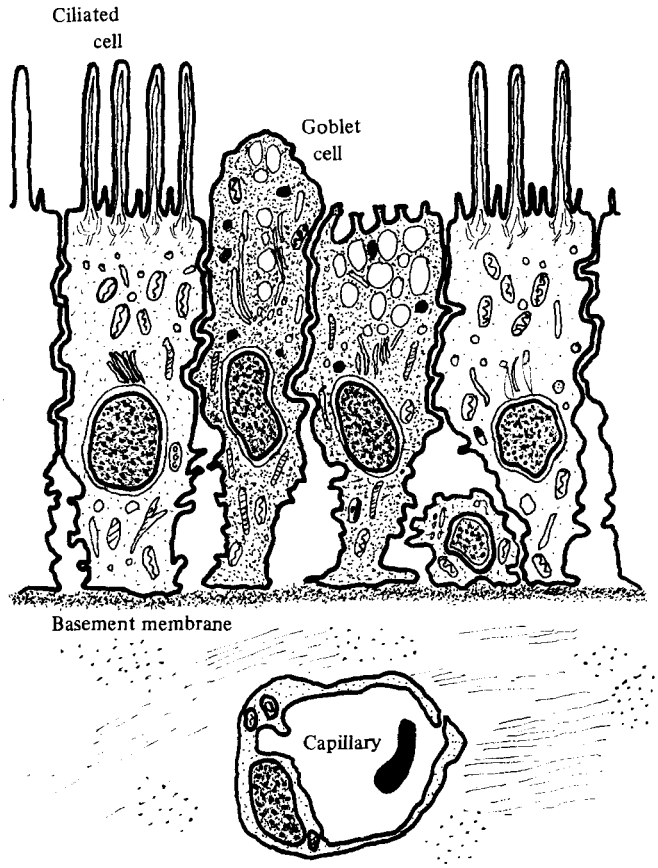

FIGURE 1. A schematic diagram of bronchial epithelium.

membrane. Below the basement membrane, the capillary layer is embedded in a layer of connective tissue. Unfortunately, there are no accurate *in vivo* measurements of serous/mucous lining which may be of the order of 5–10 μm in depth or of the distances between the epithelial surface and the capillary structures. DuBois & Rogers (1968) ignored the mucous layer and estimated the diffusion distance between the air and the bronchial capillaries to be 5% of bronchial diameter, based on inspection of bronchial cross-sections given by von Hayek (1953). These are the only published estimates of such distances known to the authors. However, the morphology

on which these estimates are based has been questioned and it is the view of others that the relevant diffusion distance is nearly constant. All calculations in the present work, however, are based on the estimates of DuBois & Rogers (table 1).

3. The model

As a first step we consider an imaginary, infinitely long airway defined by two concentric circular cylinders (a more realistic model of a branched network of airways will be considered shortly). The inner cylinder defines the flowing gas phase while the annulus is the bronchial wall, considered for convenience as a stationary homogeneous liquid rather than a tissue compartment of unknown properties. The bronchial capillary network is regarded as a continuous surface and is represented by the outer cylindrical boundary of the model.

In this work it is assumed that the injected solute is soluble in tissue, according to an approximately linear equilibrium relation at the gas-tissue interface. An initial introduction, into the flowing gas, of a slug of such solute leads to

(*a*) a net removal of solute from the gas (i.e. uptake by the bronchial wall);

(*b*) an eventual reduction in the speed of the advancing solute; and

(*c*) a spreading of the solute distribution in the gas. This dispersive process is determined by the interaction between axial convection in the gas, radial diffusion within phases and the interphase exchange of matter, and occurs in many different situations (e.g. in soil science, chromatography, physiological flows and in similar heat- and mass-transfer problems).

Aris (1959) considered this dispersion problem in terms of the method of moments but only derived large-time results. In the present paper, the Aris method is applied to determine the unsteady behaviour of the first three spatial moments of the solute distribution in the gas (corresponding to (*a*)–(*c*) above) following the introduction of a slug of the soluble material into the flow (the determination of the next time-dependent moment, which is associated with profile skewness, was not considered to be practicable owing to the formidable algebraic and computational effort required).

The results are then used to model the uptake and dispersion of a tissue-soluble gas component in a branched network of lung airways. The transition from a single, infinitely long airway model to a branched system of airways of finite length is made by following the rationale of Ultman & Blatman (1977*a*, *b*). These authors assumed that each tubular branch in the system responds like a segment of an infinitely long tube and that the tracer distribution experiences a corresponding change in variance (and, by implication, in the other moments of the distribution) during its passage. In this paper we confine our attention to changes in the spatial moments of the distribution and do not attempt to infer differences in the time variance, for example, of the solute distribution as was done by Ultman & Blatman (1977*a*, *b*) for single-phase dispersion.

4. Gas transport in the single-airway model

The convection–diffusion equations for solute in the infinitely long airway model, in terms of cylindrical coordinates (r, x) and time t, are

$$\frac{\partial c_1}{\partial t} + U(r)\frac{\partial c_1}{\partial x} = D_1\left(\frac{\partial^2 c_1}{\partial x^2} + \frac{1}{r}\frac{\partial}{\partial r}r\frac{\partial c_1}{\partial r}\right) \quad \text{in the gas} \quad (0 < r < a_1), \tag{1a}$$

$$\frac{\partial c_2}{\partial t} = D_2\left(\frac{\partial^2 c_2}{\partial x^2} + \frac{1}{r}\frac{\partial}{\partial r}r\frac{\partial c_2}{\partial r}\right) \quad \text{in the tissue} \quad (a_1 < r < a_2), \tag{1b}$$

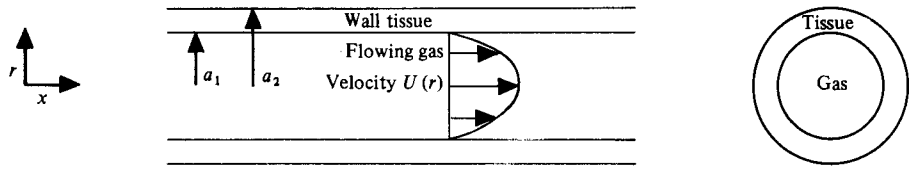

FIGURE 2. A schematic representation of a cylindrical model airway.

where $c_1(r, x, t)$ and $c_2(r, x, t)$ are solute concentrations in the gas and the tissue respectively, for which the corresponding molecular diffusion coefficients are D_1 and D_2. The radius of the inner cylinder is given by a_1 and that of the outer cylinder by a_2 (see figure 2). The axial velocity $U(r)$ of the gas is taken to be independent of x and t, and solute concentrations are assumed to be low, so velocity components induced by mass transfer between gas and tissue can be ignored. Although U is taken to be independent of x within a given airway, its magnitude will depend on the generation of branching under consideration. For example, U will be much larger in the trachea than it will be in the respiratory bronchioles.

The effective diffusivity D_2 of a soluble gas in bronchial tissue is very difficult to predict because of the complex structural and chemical composition of the wall. The diffusion of water-soluble substances will be hindered to some degree since the water component of the wall (about $\frac{1}{3}$ by weight) is bound mainly to large intercellular molecules. Similarly, the transport of highly fat-soluble materials such as benzene and anaesthetic agents, which occurs mainly via the cellular components of the wall, will depend on the true area available for diffusion. In this work we have simply chosen D_2 to be 10^{-5} cm^2/s. The value of D_1 is of the order of 10^{-1} cm^2/s.

Since $D_2 \ll D_1$, the $\partial^2 c_2/\partial x^2$ term in (1*b*) can be ignored for the purposes of predicting longitudinal dispersion in the gas phase. However, we have retained that term in our analysis as it is appropriate in other situations for which D_2/D_1 is not small.

Boundary conditions describing continuity of flux and negligible diffusion resistance at the interface $r = a_1$ are

$$D_2 \frac{\partial c_2}{\partial r}(a_1, x, t) = D_1 \frac{\partial c_1}{\partial r}(a_1, x, t), \tag{2a}$$

and the linear equilibrium isotherm is given by

$$c_2(a_1, x, t) = \beta c_1(a_1, x, t), \tag{2b}$$

where β is the solubility coefficient. Zero-flux conditions are chosen on the axis of symmetry and on the outer cylinder (i.e. it is taken to be insulating) so that $(\partial c_1/\partial r)(0, x, t) = 0$ and $(\partial c_2/\partial r)(a, x, t) = 0$. The choice of zero flux on the outer cylindrical boundary is equivalent to ignoring the uptake of solute by the bronchial blood supply. This assumption depends on the tissue thickness, diffusivity and exposure time to the soluble gas. It will be a much better approximation near generation 0 than it will near generation 16. The characteristic diffusion time in tissue $((a_2 - a_1)^2/D_2)$ varies from about 800 s at generation 0 to about 1 s at generation 16 based on tissue thickness of 5 % of airway diameter and diffusivity D_2 of 10^{-5} cm^2/s.

The linear equilibrium relation (2*b*) is applicable to the absorption of many gases in dilute concentrations. However, in the case of SO_2, for example, absorption in water is accompanied by an ionization reaction and the solubility relation is nonlinear, especially at low concentrations (Pearson *et al.* 1951). In that case, the reaction is assumed to be instantaneous and relation (2*b*) is based on an average slope over the range of solute concentrations encountered. However, this solubility model cannot

be applied to the more complicated example of NO_2 absorption, since the associated chemical equilibria in that case involve other oxides of nitrogen (Wendel & Pigford 1958).

Values of the solubility coefficient β can range from approximately zero for relatively insoluble gases (e.g. $\beta \approx 0{\cdot}01$ for helium) to as high as about 1500 for ethanol, for example. Estimated β values for SO_2 in water, obtained by approximating the equilibrium curve by a straight line between the origin and the point of maximum concentration, vary roughly from about 750 for SO_2 burdens of 10 p.p.m. in air to about 90 for maximum air levels of 1000 p.p.m. At larger SO_2 concentrations, β approximates a constant value of about 20, corresponding to the increased dominance of un-ionized SO_2 in the absorbed gas.

It is most convenient to pose the problem in terms of dimensionless variables

$$X = \frac{D_1 x}{U_0 a_1^2}, \quad y = \frac{r}{a_1}, \quad \tau = \frac{D_1 t}{a_1^2}, \quad W = \frac{U}{U_0},$$

$$C_i(y, X, \tau) = \frac{c_i(r, x, t)}{c_0}, \quad Pe = \frac{U_0 a_1}{D_1}, \quad \lambda = \frac{D_2}{D_1}, \quad b = \frac{a_2}{a_1},$$

where U_0 and c_0 are reference values of U and c_i respectively. In terms of these variables, the transport equations become

$$\frac{\partial C_1}{\partial \tau} + W(y)\frac{\partial C_1}{\partial X} = \frac{1}{y}\frac{\partial}{\partial y}\left(y\frac{\partial C_1}{\partial y}\right) + \frac{1}{Pe^2}\frac{\partial^2 C_1}{\partial X^2} \quad (0 < y < 1), \tag{3a}$$

$$\frac{\partial C_2}{\partial \tau} = \lambda\left(\frac{1}{y}\frac{\partial}{\partial y}\left(y\frac{\partial C_2}{\partial y}\right) + \frac{1}{Pe^2}\frac{\partial^2 C_2}{\partial X^2}\right) \quad (1 < y < b), \tag{3b}$$

with boundary conditions

$$\begin{aligned} \frac{\partial C_1}{\partial y}(0, X, \tau) &= \frac{\partial C_2}{\partial y}(b, X, \tau) = 0, \\ C_2(1, X, \tau) &= \beta C_1(1, X, \tau), \\ \frac{\partial C_1}{\partial y}(1, X, \tau) &= \lambda \frac{\partial C_2}{\partial y}(1, X, \tau). \end{aligned} \tag{4}$$

Following Aris (1959), we set

$$C_i^{(p)}(y, \tau) = \int_{-\infty}^{\infty} X^p C_i(y, X, \tau)\, dX, \tag{5}$$

where it is assumed that $X^p C_i \to 0$ as $X \to \pm\infty$ for all p. In this analysis the coordinate axes are fixed. The transformation to coordinates moving with the centroid of the solute distribution carried out in the steady-state analysis by Aris is not convenient here since the centroid velocity is now time-dependent. In terms of the $C_i^{(p)}$, (3*a*) and (3*b*) become

$$\frac{\partial C_1^{(p)}}{\partial \tau} = \frac{1}{y}\frac{\partial}{\partial y}\left(y\frac{\partial C_1^{(p)}}{\partial y}\right) + W(y)\, pC_1^{(p-1)} + \frac{p(p-1)}{Pe^2}C_1^{(p-2)} \quad (0 < y < 1), \tag{6a}$$

$$\frac{\partial C_2^{(p)}}{\partial \tau} = \lambda\left(\frac{1}{y}\frac{\partial}{\partial y}\left(y\frac{\partial C_2^{(p)}}{\partial y}\right) + \frac{p(p-1)}{Pe^2}C_2^{(p-2)}\right) \quad (1 < y < b), \tag{6b}$$

with boundary conditions

$$\frac{\partial C_1^{(p)}}{\partial y}(0,\tau) = \frac{\partial C_2^{(p)}}{\partial y}(b,\tau) = 0,$$

$$C_2^{(p)}(1,\tau) = \beta C_1^{(p)}(1,\tau), \quad \frac{\partial C_1^{(p)}}{\partial y}(1,\tau) = \lambda \frac{\partial C_1^{(p)}}{\partial y}(1,\tau).$$

These equations may also be obtained from equations (6) in the Aris paper. The objective is to determine $C_i^{(p)}$ $(p = 0, 1, 2)$, and hence the spatial moments defined by

$$m_1^{(p)}(\tau) = 2\int_0^1 y C_1^{(p)}(y,\tau)\,dy, \tag{7a}$$

$$m_2^{(p)}(\tau) = \frac{2}{b^2-1}\int_1^b y C_2^{(p)}(y,\tau)\,dy. \tag{7b}$$

with particular attention focused on the moments $m_1^{(p)}(\tau)$ of the distribution in the gas. The solution for general initial conditions and for the special case of a pulse injection is given in appendix A.

The solute distribution in the gas has the following dimensional properties in terms of the moments:

$$\text{amount of solute in the gas} = c_0 \pi a_1^3 Pe\, m_1^{(0)}(\tau), \tag{8a}$$

$$\text{velocity } U_g \text{ of the centre of mass} = U_0\left(\frac{m_1^{(1)}}{m_1^{(0)}}\right)', \tag{8b}$$

$$\text{mixing coefficient } D_g = \frac{1}{2}\frac{d\sigma^2}{dt} = \tfrac{1}{2}D_1 Pe^2\left(\frac{m_1^{(2)}}{m_1^{(0)}} - \left(\frac{m_1^{(1)}}{m_1^{(0)}}\right)^2\right)', \tag{8c}$$

where σ^2 is the variance of the distribution and $'$ represents differentiation with respect to dimensionless time τ. The coefficient D_g is analogous to an effective dispersion coefficient whose use in a dispersion model based on Fick's law requires that an initial impulse of the radially averaged concentration distribution develops approximately as a Gaussian function of axial distance. Although this requirement is not met in general for isolated tubes, and conditions for which it may be satisfied within the lung are not clear, the mixing coefficient remains useful as an index of the rate of solute spreading.

We now confine our attention to Poiseuille flow and to solute distributions which are initially zero in the tissue and radially uniform in the gas phase. Since our equations (6) and their boundary conditions are invariant under the transformation

$$C_i^{*(p)} = \sum_{r=0}^{p} \frac{p!}{(p-r)!} A_r C_i^{(p-r)},$$

it is possible to choose the constants A_0, A_1 and A_2 to transform the problem of determining $m_1^{(0)}(\tau)/m_1^{(0)}(0)$, U_g and D_g (which are also invariant under the transformation) to one in which

$$C_1^{*(0)}(y,0) = 1, \quad C_2^{*(0)}(y,0) = 0, \quad C_i^{*(p)}(y,0) = 0 \quad (p > 0, \quad i = 1,2),$$

independently of the initial axial distribution of solute in the gas phase. It is therefore sufficient to consider a pulse of solute introduced into the Poiseuille flow (dimensionless velocity $W = 1-y^2$) at time $\tau = 0$ such that $C_1(y, X, 0) = \delta(X)$ and $C_2(y, X, 0) = 0$ (the solution details are given in appendix A).

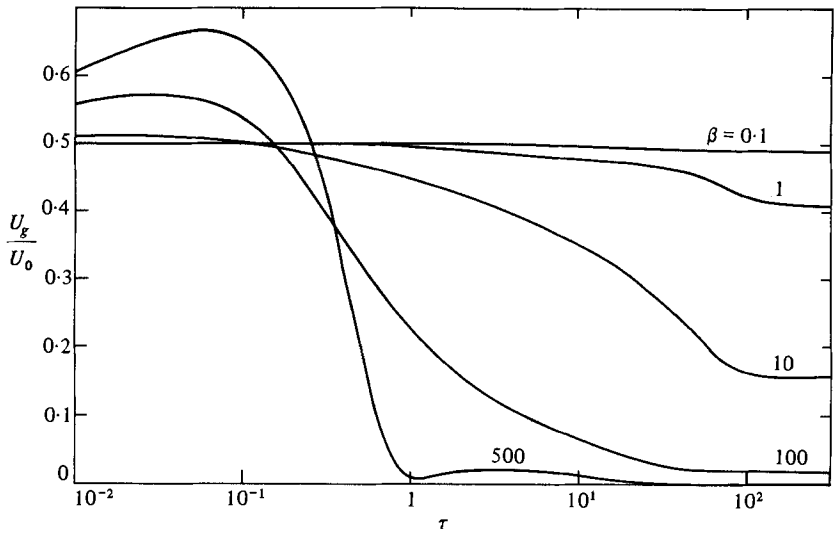

FIGURE 3. Dimensionless velocity of the centre of mass of the solute distribution in the infinitely long airway model versus dimensionless time $\tau = D_1 t/a_1^2$ for $\lambda = 10^{-4}$ and $b = 1{\cdot}1$, assuming Poiseuille flow and a solute distribution which is initially zero in the tissue and radially uniform in the gas.

At $\tau = 0$, the velocity U_g of the solute centre of mass in the gas equals $\frac{1}{2}U_0$, the mean velocity of the bulk axial flow. Velocity U_g then increases initially as solute is removed from the slow-moving fluid near the interface, thereby weighting the solute distribution in favour of the faster-moving central portion. In figure 3, this initial rise is only evident for values of β (solubility coefficient) larger than about 10. For larger values of dimensionless time τ, U_g reduces to the value $\frac{1}{2}U_0 R$ where $R = 1/(1+(b^2-1)\beta)$ is the steady-state solute fraction in the gas.

Littlewood (1970) has discussed the mechanisms of the exchange process between a mobile and a stationary phase, corresponding to large times. As the solute distribution in the gas phase moves forward, transverse corrective fluxes are generated which remove solute to the tissue at the front and unload solute into the gas at the rear. This accounts for the reduced value of U_g.

Factors that contribute to longitudinal dispersion include the relative amounts of solute in each phase (partition effect), radial diffusion in the gas (Taylor-type dispersion effects), radial diffusion in the tissue, and axial molecular diffusion. At large times the overall effect is for dispersion to be greater than it would be in the absence of exchange ($\beta = 0$), except when β is large and the solute fraction in the gas is small.

The partition effect decreases dispersion of solute in the gas with increasing solute fraction in the tissue phase. Longitudinal dispersion is delayed as the tissue temporarily captures gas molecules, the delay increasing with solubility. To illustrate, suppose that the solute concentrations in the gas and tissue were uniform and in equilibrium; an axial diffusivity D in the gas then reduces to an effective diffusivity of $D/(1+(b^2-1)\beta)$.

If transverse diffusion in the gas and tissue were infinitely rapid then no dispersion (apart from partition-modified axial molecular diffusion) would occur. Allowing for the finite time for radial diffusion of solute in the gas results in a dispersion process of the type described by Taylor (1953), in which convective spreading is modified by radial diffusion. However, this effect of radial diffusion is inhibited by interphase solute exchange which tends to maintain radial concentration gradients. Thus the

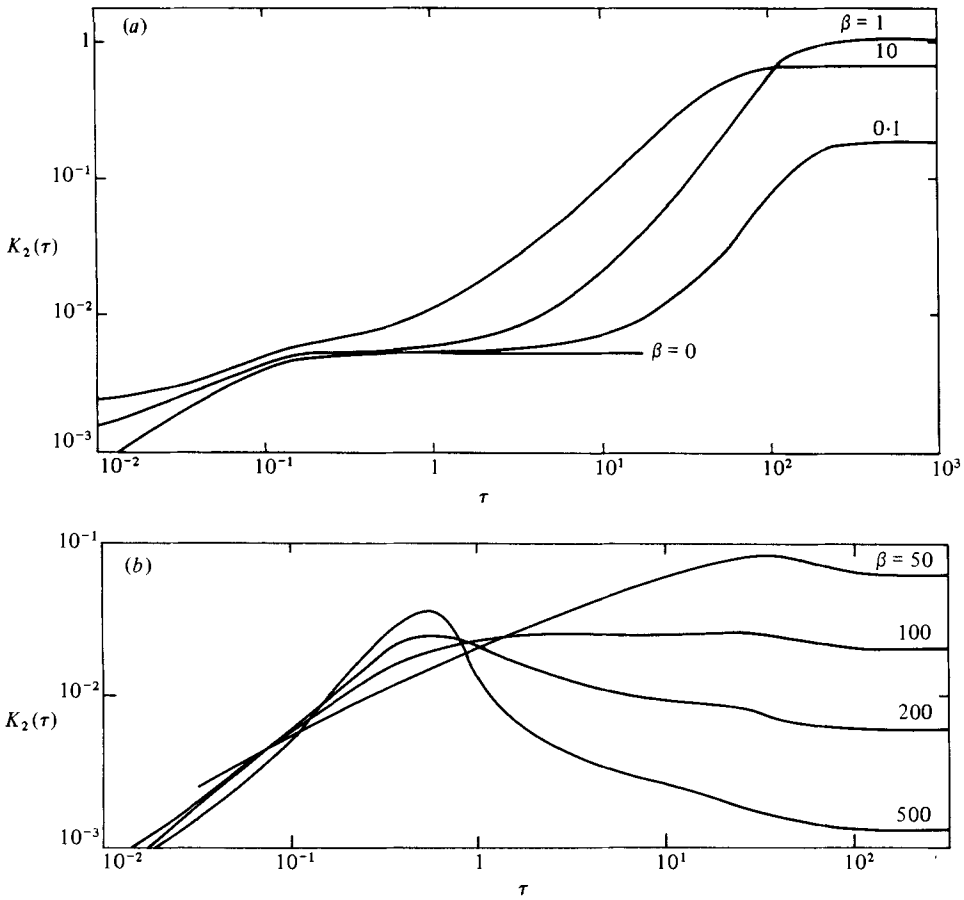

FIGURE 4. Plot of $K_2(\tau)$ versus dimensionless time $\tau = D_1 t/a_1^2$ for $\lambda = 10^{-4}$ and $b = 1{\cdot}1$ in the infinitely long airway model where the mixing coefficient $D_g \approx D_1 Pe^2 K_2(\tau)$ when Pe is large. Poiseuille flow is assumed and the solute distribution is taken to be initially zero in the tissue and radially uniform in the gas.

Taylor-type dispersion component is expected to be greater in the presence of exchange than in its absence. Including the finite rate of diffusion across the tissue phase introduces a contribution to dispersion by delaying the exchange process. As solute moves forward in the gas and interphase exchange occurs, the front portion travels further through the gas and solute at the rear remains longer in the tissue than it would if transverse diffusion in the tissue were instantaneous.

The unsteady mixing coefficient D_g given by (8*c*) may be written in the form

$$D_g = D_1(K_1(\tau) + Pe^2 K_2(\tau)),$$

where K_1 and K_2 are independent of Pe (and concentration). In the absence of flow, axial spreading by molecular diffusion will be reduced according to the partition effect. In terms of the exchange process, transverse corrective fluxes are induced which tend to sharpen the peak and erode the sides of the developing solute distribution. In that case, $D_g = D_1 K_1(\tau)$, where $K_1(\tau)$ is expected to decrease with time from an initial value of 1 toward some steady value.

Conversely, when Pe is large, axial molecular diffusion can be ignored and $D_g \approx D_1 Pe^2 K_2(\tau)$. The coefficient K_2 is plotted as a function of τ in figures 4(*a*, *b*).

The steady-state values of K_2 are based on the Aris (1959) result given in appendix B (equation (B 13)). In figure 4(*a*) the partition effect is not sufficient to prevent the increase in K_2 with time. When $\beta = 0{\cdot}1$, the K_2 curve initially follows that for $\beta = 0$ until the onset of exchange effects, after which it rises rapidly towards its steady value. As β increases, the K_2 curve in figures 4(*a*, *b*) at first rises before falling at both the large- and small-time extremes. Indeed, if β is sufficiently large ($\beta > 200$), the large- and small-time values of K_2 fall below the corresponding $\beta = 0$ values; presumably the partition effect dominates at these times.

Our discussion of figures 3 and 4 has focused on the short-and long-time trends. Indeed, we are unable to interpret physically the details of these figures at intermediate times (e.g. the sharp changes in slope in figure 3 at $\tau \approx 100$ for $\beta = 1$ and 10 or the hump between $\tau = 1$ and 10 for $\beta = 500$) in the absence of a more detailed knowledge of the corresponding concentration changes along the tube. Unfortunately, a full numerical solution is required to predict the concentration at times that are neither asymptotically large nor small. Furthermore, our analysis does not reveal any means of isolating expressions for the various factors contributing to dispersion, suggesting a complex interaction.

5. Branched-network model

By following the rationale of Ultman & Blatman (1977*a*, *b*), we now use the above results for the infinitely long airway model to construct a more realistic model of transport in a (symmetrical and rigid) branching network of airways. The complex flow profiles characteristic of branched systems (Pedley *et al.* 1977) are ignored, and each branch of the system is presumed to respond like a segment of an infinitely long tube (airway) in which the flow is fully developed. A corresponding change in the tracer distribution is assumed to occur during its passage through each segment.

Ultman & Blatman adopted this approach for tracers which remained in the gas phase and inferred mixing coefficients for branching systems using the corresponding time-dependent form of the effective axial dispersion coefficient in fully developed laminar tube flow (Gill & Sankarasubramanian 1970). They found that the data of Scherer *et al.* (1975) for a five-generation glass model were consistent with the assumption that the concentration profile develops continuously through the branched network during inspiration and that it undergoes redevelopment within each branch during expiration.

Let $j = 0, 1, 2, \ldots$ denote the generations of branching in a symmetric lung in which the trachea is given by $j = 0$. Define the dimensionless residence time of solute in the gas reaching the end of the ith generation as

$$\tau_i = \sum_{j=0}^{i} \Delta\tau_j,$$

where the $\Delta\tau_j$ are determined by solving the following expression progressively for τ_j given τ_{j-1}:

$$\frac{a_{1j}^2}{D_1} \int_{\tau_{j-1}}^{\tau_j} U_g \, d\tau = l_j,$$

for which a_{1j} and l_j are respectively the radius and length of a tube in the jth generation. That is, the progress of the slug is determined by the movement of its centre of mass. Applying (8*b*) now gives

$$\left(\frac{m_1^{(1)}}{m_1^{(0)}}\right)_{\tau=\tau_j} - \left(\frac{m_1^{(1)}}{m_1^{(0)}}\right)_{\tau=\tau_{j-1}} = \frac{D_1 l_j}{2\bar{U}_j a_{1j}^2}, \tag{9}$$

where $\overline{U}_j$ is the mean axial velocity (half the peak velocity of the assumed parabolic flow). Note that, in the spirit of Ultman & Blatman, the integration is taken over dimensionless time.

When the centre of mass reaches the end of the $(j-1)$th generation, the system is assumed to change immediately to that of 2^j-parallel, infinitely long tubes, each having the diameter corresponding to that new generation of airways. The shape of the concentration distributions in the $(j-1)$th generation is assumed to be unaltered when the transition is made to the jth generation, but the concentrations are scaled by a factor to ensure that the total amount of solute in the system remains unchanged. That is, no mixing is assumed during the transition and the concentration profile is allowed to develop continuously, corresponding to Ultman & Blatman's recommendation for modelling inspiration. On this basis, the loss of solute from the gas in all tubes of the jth generation, expressed as a fraction of the initial amount introduced, is given by

$$\Delta\text{uptake} = \frac{m_1^{(0)}(\tau_{j-1}) - m_1^{(0)}(\tau_j)}{m_1^{(0)}(0)}. \tag{10}$$

We define here an index H of the uptake efficiency of the bronchial wall as the ratio of the uptake rate to the amount of solute in the gas phase. For an infinitely long airway

$$H = \frac{-D_1}{a_1^2}\frac{(m_1^{(0)}(\tau))'}{m_1^{(0)}(\tau)}$$

from (8a). To estimate the uptake efficiency of the bronchial wall in the jth generation of the branching-lung model, we again average over the dimensionless residence time of the solute to obtain

$$\overline{H} = \frac{D_1}{a_1^2\,\Delta\tau_j}\log\frac{m_1^{(0)}(\tau_{j-1})}{m_1^{(0)}(\tau_j)}. \tag{11}$$

Similarly, a time-averaged mixing coefficient for the jth generation is taken to be

$$\overline{D}_g = \frac{1}{\Delta\tau_j}\int_{\tau_{j-1}}^{\tau_j} D_g\,d\tau,$$

where D_g is given by (8c).

From (9), the dimensionless time increment $\Delta\tau_j$, and hence the uptake fraction given by (10), is independent of airway radius a_{1j} at constant flow rate $(2^j\overline{U}_j\pi a_{1j}^2)$. Consequently the uptake pattern predicted by the model is unaffected by bronchoconstriction acting uniformly between parallel pathways, although the uptake efficiency given by (11) will increase. Although flow passes more quickly through such a constricted airway, and the area of the air–tissue interface is smaller, the uptake rate is greater for a given initial injected amount of solute since radial concentration differences are larger (the concentration scaling factor for that generation is larger) and also the radial coordinate is contracted.

The effect of progressive uptake of solute in the branching lung model is demonstrated for different solubility coefficients (figure 5) and different flow rates (figure 6). As was expected, the lower the gas solubility, the greater is the penetration of solute into the model and the greater the amount of solute in the gas phase at any time. For example, after a 1 s inspiration at a flow rate of 20 l/min, the centre of mass of the solute distribution has reached the end of the 10th and 15th generations of branching for $\beta = 500$ and $\beta = 25$, respectively (figure 5a). The corresponding solute fractions in the airways are then 1 % and 18 % of the initial amounts inhaled.

In figure 5(b) uptake and the residence time are shown for each generation. For fixed flow rate, solute residence time within an airway depends on solubility (figure

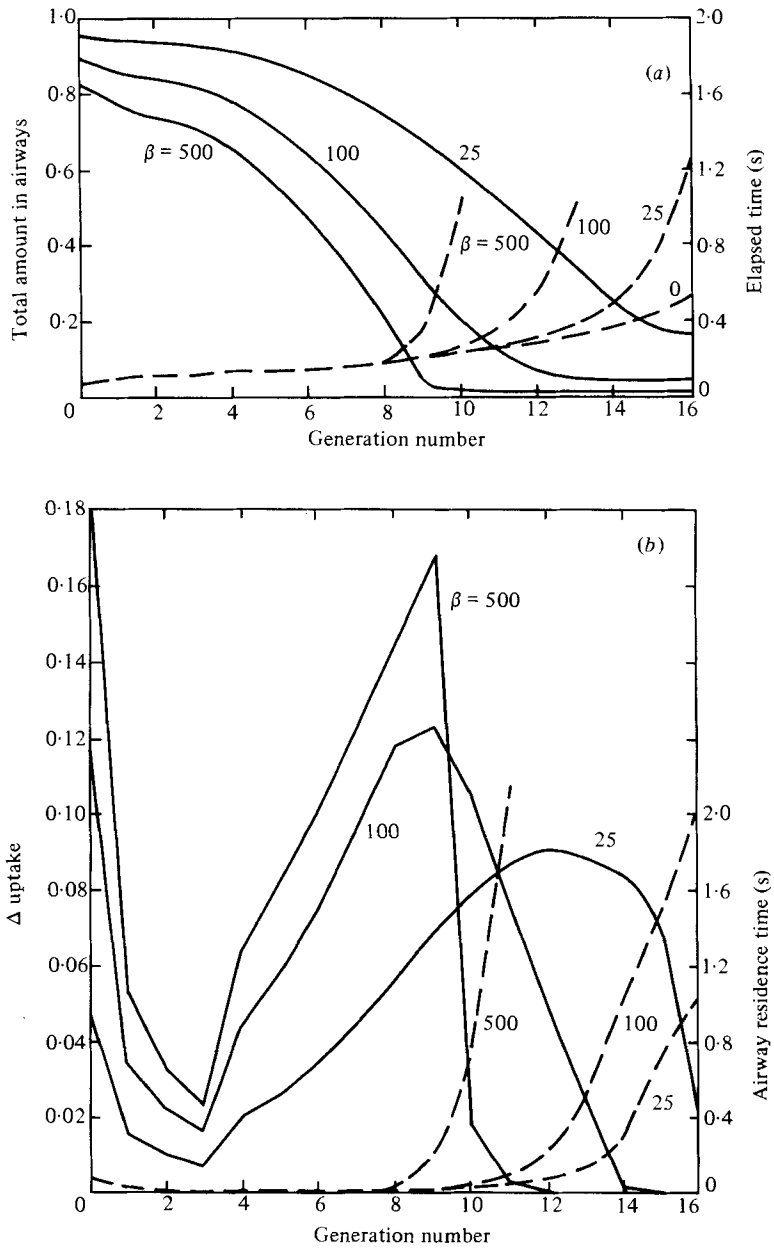

FIGURE 5. The amount of solute in all airways of the branching-lung model, expressed as a fraction of the initial amount injected at the model entrance, is calculated when the solute centre of mass has reached the end of a generation. In (*a*) it is plotted versus generation number (solid lines), with the dashed lines representing the corresponding elapsed time. In (*b*) the solute fraction (Δuptake), extracted as the solute centre of mass passes through the airways of a given generation, is plotted versus generation number (solid lines), with the dashed lines representing the corresponding residence times. The simulations correspond to the inhalation of a solute pulse at a constant flow rate F of 20 l/min, with $D_1 = 0{\cdot}1$ cm^2/s, $D_2 = 10^{-5}$ cm^2/s and $b = 1{\cdot}1$, for solubility coefficients $\beta = 25$, 100 and 500. Poiseuille flow in each airway is assumed and the solute distribution is taken to be initially zero in the tissue and radially uniform in the gas.

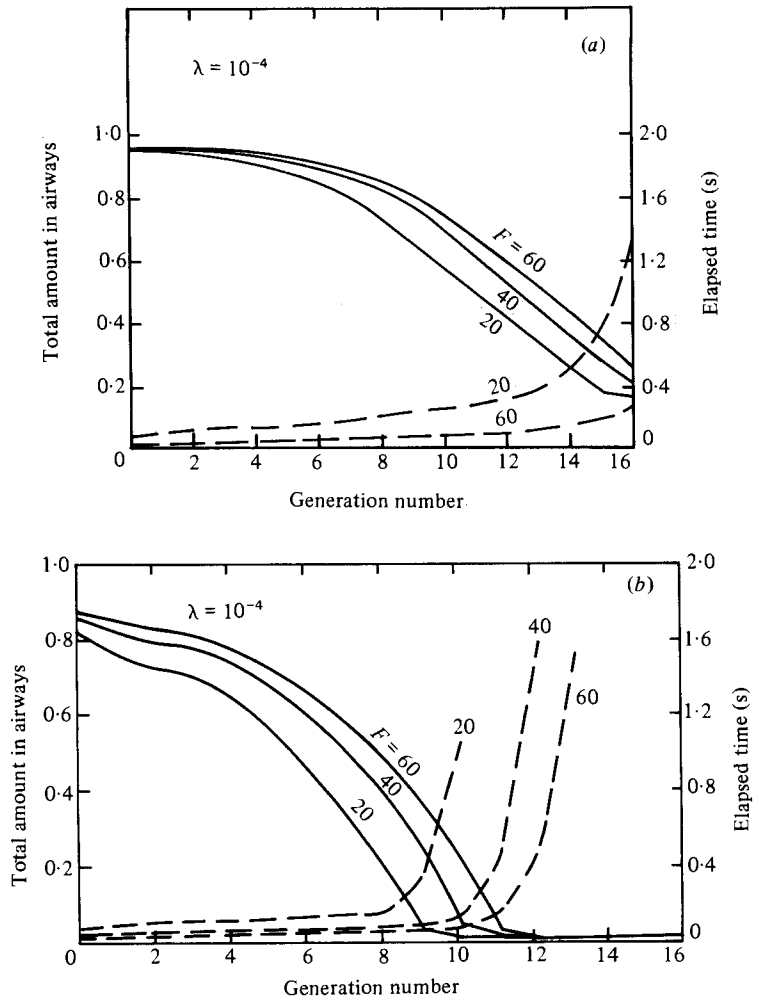

FIGURE 6. The amount of solute in all airways of the branching lung model, expressed as a fraction of the initial amount injected at the model entrance, is calculated when the solute centre of mass has reached the end of a generation. It is plotted versus generation number (solid lines), with the dashed lines representing the corresponding elapsed times. The simulations correspond to the inhalation of a solute pulse at constant flow rates F of 20, 40 and 60 l/min, with $D_1 = 0{\cdot}1$ cm^2/s, $D_2 = 10^{-5}$ cm^2/s and $b = 1{\cdot}1$, for solubility coefficients (*a*) $\beta = 25$ and (*b*) $\beta = 500$. Poiseuille flow in each airway is assumed and the solute distribution is taken to be initially zero in the tissue and radially uniform in the gas.

3), airway length and the total cross-sectional area at the given level of branching. Residence time falls progressively in generations 0–3, corresponding to the drop in airway length with a roughly constant-area cross-section (table 1). From generations 3–8 airway residence time is almost constant (however, dimensionless $\Delta\tau_j$ increases with generation owing to the falling airway diameter), after which it rises at a rate which increases with solubility.

The incremental uptake fraction (Δuptake) depends on both the solubility and the dimensionless airway-residence time. Corresponding to the latter, Δuptake falls in generations 0–3 and subsequently rises. It attains a maximum before falling to zero as gas-tissue exchange approaches a steady state. In figure 5(*b*) the location of the maximum is the same (generation 9) for $\beta = 100$ and 500, whereas for $\beta = 25$ it occurs

at generation 12. Furthermore, the size of the maximum appears to increase with increasing solubility. The point of zero Δuptake (i.e. when solute losses at the front of the bolus are balanced by back-diffusion at the rear) is located deeper in the model lung for lower-solubility solutes (in particular, at generations 12 and 15 for $\beta = 500$ and 100 respectively in figure 5*b*).

Apart from increasing the penetration of the solute centre of mass over a given period of inspiration, increasing the flow rate either reduces or has no effect on the predicted overall uptake, depending on the solubility and the level of branching at which the comparison is made; this result is consistent with the observations of Ichioka (1972). For example, when $\beta = 25$ (figure 6*a*), the cumulative uptake in generations 0–16 falls with increasing flow rate. Alternatively, when $\beta = 500$ (figure 6*b*), it falls in generations 0–10 with increasing flow rate but is unaffected distal to generation 11.

The uptake efficiency index $\bar{H}$ for each generation consistently increases with flow rate for $\beta = 25$ and 500 (figure 7), a result which agrees qualitatively with the observations of Aharonson *et al.* (1974). Like Δuptake in figure 5, $\bar{H}$ rises to a maximum corresponding to the increase in the dimensionless residence time, and subsequently falls with the approach of steady-state solute exchange. The rise and fall in $\bar{H}$ is more rapid at the higher solubility, with the result that, in generations 0 to 10–12, $\bar{H}$ for $\beta = 500$ is greater than it is for $\beta = 25$, whereas in subsequent generations $\bar{H}$ is greater for $\beta = 25$.

In figure 8, the mean mixing coefficient $\bar{D}_g$ is plotted against generation number for a flow rate of 20 l/min. As for the non-soluble case ($\beta = 0$), $\bar{D}_g$ decreases with increasing generation, corresponding to the fall in axial velocity with distance into the lung. Over the range of solubilities considered ($\beta = 0$–500), $\bar{D}_g$ has the same order of magnitude at each of generations 1–7, but thereafter lies above or below the zero-solubility case, depending on the value of β and the generation number. For each of $\beta = 25$, 100 and 500 there is a point at which $\bar{D}_g$ becomes less than the value for molecular diffusion in the gas phase. That point lies more proximally with increasing β.

6. Discussion of model assumptions

Because of the complexity of the human lung, it can be seen that many drastic assumptions have been made so that some analytical progress can be achieved. Consequently, an important question is whether our model provides a realistic description of dispersion and absorption in such a physiologically, morphologically, chemically and dynamically complex system. Unfortunately, there is no clear data on the distribution of uptake with which to compare our predictions.

The major assumptions made above are:

(i) the lung consists of a symmetrical branching airway system;

(ii) fully developed Poiseuille flow occurs in all airways;

(iii) each airway is modelled as a finite section of an infinite tube;

(iv) local dispersion characteristics are unaffected by airway junctions;

(v) the wall cellular and connective tissue are modelled as a stationary homogeneous liquid:

(vi) linear solubility relations are used.

We may consider the acceptability of these assumptions in order.

(i) Models of flow into the lung are usually symmetric even though the branching pattern is really asymmetric. Weibel's model is commonly used, although it is well

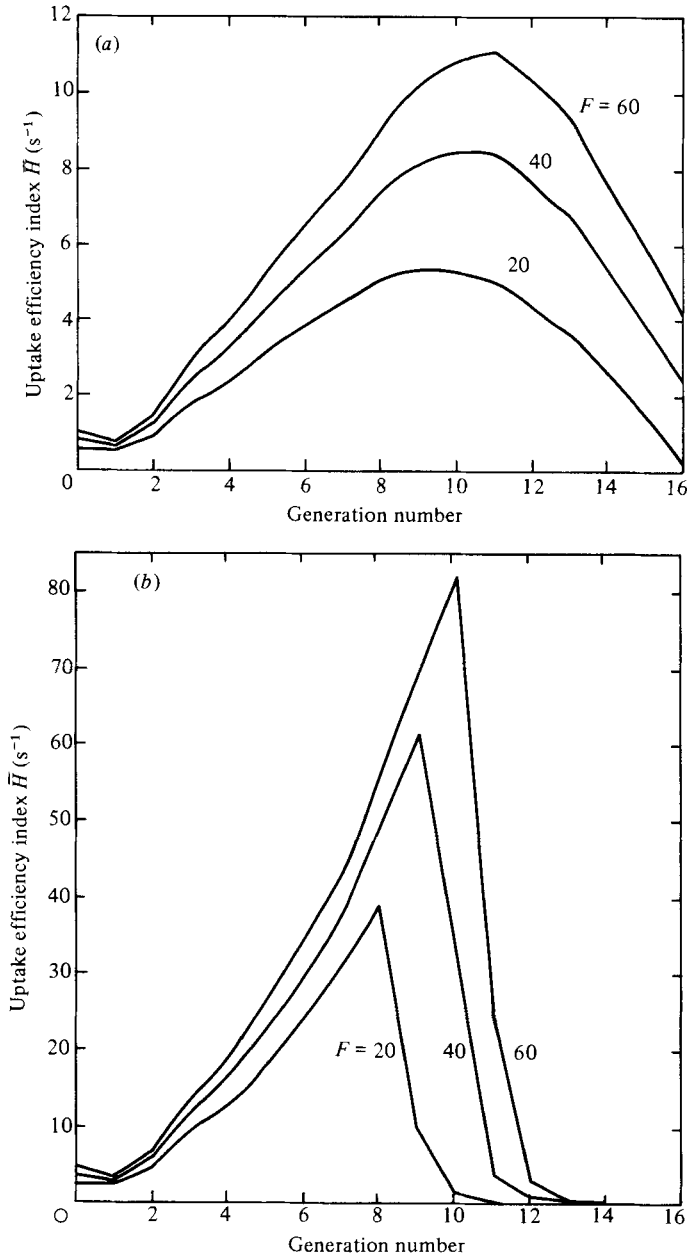

FIGURE 7. Uptake efficiency index $\bar{H}$ estimated for a given generation of branching versus generation number. Results are based on simulations corresponding to the inhalation of a solute pulse at constant flow rates F of 20, 40 and 60 l/min, with $D_1 = 0{\cdot}1$ cm^2/s, $D_2 = 10^{-5}$ cm/s and $b = 1{\cdot}1$, for solubility coefficients (*a*) $\beta = 25$ and (*b*) $\beta = 500$. Poiseuille flow in each airway is assumed and the solute distribution is taken to be initially zero in the tissue and radially uniform in the gas.

known that the data on which it is based is firstly limited and secondly derived in different ways – large airways directly measured, small airways statistically measured, and a patching in between. Asymmetric models such as those of Horsfield & Cumming are difficult to use since the many different pathways though the network must be considered separately, unlike symmetric models in which all such pathways are

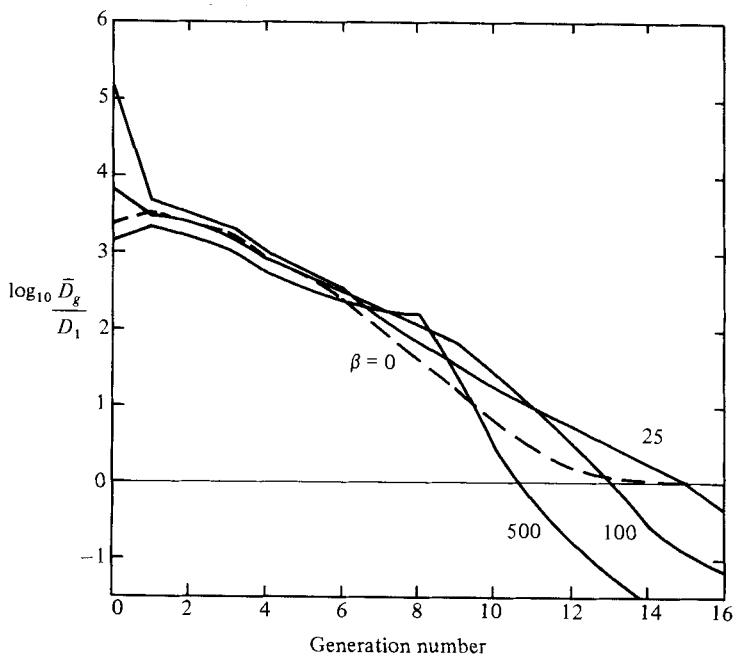

FIGURE 8. The mixing coefficient $\bar{D}_g$ estimated for a given generation of branching plotted as $\log_{10}(\bar{D}_g/D_1)$ versus generation number. Results are based on simulations corresponding to the inhalation of a solute pulse at a constant flow rate F of 20 l/min, with $D_1 = 0{\cdot}1$ cm^2/s, $D_2 = 10^{-5}$ cm^2/s and $b = 1{\cdot}1$, for solubility coefficients $\beta = 0$, 25, 100 and 500. Poiseuille flow in each airway is assumed and the solute distribution is taken to be initially zero in the tissue and radially uniform in the gas.

identical. Further, the prediction of flow within the individual airways of an asymmetric model requires additional assumptions about the rate of volume change of the airspace subtended at each junction. Indeed, the question of asymmetry in the lung, and its consequence, is itself a complex one and the subject of separate investigations.

(ii)–(iv) These three assumptions form an essential part of Ultman & Blatman's compartmental dispersion model, on which our approach is based. Ultman & Blatman found that their model predictions compared very well with the observed impulse responses of tracer gases in two- and five-generation symmetric networks over a range of flow rates. They concluded that velocity-profile distortion and secondary flows occurring at airway junctions make only a small contribution to the overall longitudinal mass transport. Thus, although these assumptions are unrealistic with regard to the flow itself, they seem sufficient for a valid description of longitudinal dispersion and therefore acceptable in the context of the present work.

Although the boundary-layer models of flow in the lung (Pedley *et al.* 1977) are necessary for predicting dynamic quantities such as pressure changes within the airways, Poiseuille flow has the essential features to consider qualitatively differential dispersion and absorption within the lung. These include a variable velocity across the airway, allowing a 'tongue' of solute to penetrate the airways together with an 'altered' profile at each junction. Of course, in any real airway the shape of the 'tongue' will be different, but the mechanisms will remain the same.

(v) There have been few measurements of diffusion across either airway walls or arterial vessels: one must therefore guess the corresponding diffusion coefficients. Studies of diffusion across the arterial wall suggest that molecules behave normally,

unless they are metabolically active in the wall (e.g. Kirk & Laursen 1955; Davis *et al.* 1981). However, there is virtually no information on the geometric hindrance effects of the interstitial matrix material. We therefore assume for the purpose of this work that the wall is homogeneous and that D_2 is in the region of the free solution value – perhaps reduced by an order of magnitude to allow for tortuosity and any trapping effects. The anticipated effect of decreasing D_2 is to increase the longitudinal penetration of solute.

(vi) As indicated earlier, a linear solubility relation may be applied to the absorption of many gases in low concentrations. This is certainly true when absorption is a purely physical process, but it also applies when the absorbed gas forms non-volatile products of instantaneous first-order reversible reactions. If such reactions are of higher order so that the solubility relation is nonlinear, a first approximation is to apply the theory based on an average solubility over the range of concentrations encountered. Our theory has not been applied to situations when reactions are not instantaneous or when they are irreversible, although similar analysis should be possible if such reactions are also first order.

This work was supported in part by the Winston Churchill Memorial Trust by the award (to M.R.D) of a Churchill Fellowship.

Appendix A. Solution procedure

It is convenient to define

$$G_i^{(p)}(y,\tau) = C_i^{(p)}(y,\tau) - C_{i\infty}^{(p)}(y,\tau) \quad (i = 1,2),$$

where the steady-state solution $C_{i\infty}^{(p)}$ satisfies our equations (6) and can be determined to within constants which depend on the initial conditions. The corresponding steady-state moments $m_{i\infty}^{(p)}$ are related to the $C_{i\infty}^{(p)}$ by (7). Aris (1959) considered the steady-state problem for a single set of moments defined to include solute in both the inner tube (gas phase) and the annulus (tissue phase).

When $p = 0$, (6*a*, *b*) are satisfied when

$$G_1^{(0)}(y,\tau) = \sum_{m=1}^{\infty} A_m \exp(-\mu_m^2 \tau) J_0(\mu_m y), \tag{A 1}$$

$$G_2^{(0)}(y,\tau) = \beta \sum_{m=1}^{\infty} A_m \exp(-\mu_m^2 \tau) M_0(\bar{\mu}_m y), \tag{A 2}$$

where $\bar{\mu}_m = \lambda^{-\frac{1}{2}}\mu_m$ and M_0 is a linear combination of Bessel functions J_0 and Y_0. The boundary conditions require that

$$J_0(\mu_m) = M_0(\mu_m), \quad J_1(\mu_m) = \beta\lambda^{\frac{1}{2}} M_1(\bar{\mu}_m), \quad M_1(\bar{\mu}_m b) = 0,$$

so that the eigenvalue equation is

$$\begin{aligned} &J_1(\mu_m)\,(Y_1(\bar{\mu}_m b)\,J_0(\bar{\mu}_m) - J_1(\bar{\mu}_m b)\,Y_0(\bar{\mu}_m)) \\ &\quad - \beta\lambda^{\frac{1}{2}} J_0(\mu_m)\,(Y_1(\bar{\mu}_m b)\,J_1(\bar{\mu}_m) - J_1(\bar{\mu}_m b)\,Y_1(\bar{\mu}_m)) = 0 \end{aligned} \tag{A 3}$$

and the function M_0 is given by

$$M_0(\bar{\mu}_m y) = P_m J_0(\bar{\mu}_m y) + Q_m Y_0(\bar{\mu}_m y), \tag{A 4}$$

where

$$\begin{aligned} P_m &= \tfrac{1}{2}\pi\bar{\mu}_m(\beta^{-1}\lambda^{-\frac{1}{2}} J_1(\mu_m)\,Y_0(\bar{\mu}_m) - J_0(\mu_m)\,Y_1(\bar{\mu}_m), \\ Q_m &= \tfrac{1}{2}\pi\bar{\mu}_m(J_0(\mu_m)\,J_1(\bar{\mu}_m) - \beta^{-1}\lambda^{-\frac{1}{2}} J_0(\bar{\mu}_m)\,J_1(\mu_m)). \end{aligned}$$

The orthogonality relation for the eigenfunctions is given by

$$I_{mn} = \left\{ \begin{array}{ll} \frac{1}{2}\beta b^2 M_0^2(\bar{\mu}_m b) + \frac{1}{2}((1-\beta) J_0^2(\mu_m) + (1-\beta^{-1}\lambda^{-1}) J_1^2(\mu_m)) & (m = n), \\ 0 & (m \neq n), \end{array} \right\} \quad \text{(A 5)}$$

where

$$I_{mn} = \int_0^1 y J_0(\mu_n y) J_0(\mu_m y)\, dy + \beta \int_1^b y M_0(\bar{\mu}_m y) M_0(\bar{\mu}_n y)\, dy.$$

Also

$$\int_0^1 y J_0(\mu_m y)\, dy = -\beta \int_1^b y M_0(\bar{\mu}_m y)\, dy = \frac{J_1(\mu_m)}{\mu_m}. \quad \text{(A 6)}$$

Hence the expression for the coefficients A_m in terms of the initial conditions is

$$A_m = \frac{1}{I_{mm}} \left(\int_0^1 y J_0(\mu_m y) C_1^{(0)}(y, 0)\, dy + \int_1^b y M_0(\bar{\mu}_m y) C_2^{(0)}(y, 0)\, dy \right), \quad \text{(A 7)}$$

after noting that $C_{2\infty}^{(0)} = \beta C_{1\infty}^{(0)}$ is a constant (see appendix B). When $p > 0$ we find that

$$G_1^{(p)}(y, \tau) = B_{p0}(\tau) + \sum_{n=1}^{\infty} B_{pn}(\tau) J_0(\mu_n y), \quad \text{(A 8)}$$

$$G_2^{(p)}(y, \tau) = \beta (B_{p0}(\tau) + \sum_{n=1}^{\infty} B_{pn}(\tau) M_0(\bar{\mu}_n y)), \quad \text{(A 9)}$$

where, after substituting into (6a, b) and applying the orthogonality relations (A 5) and (A 6).

$$B_{p0}(\tau) = -\frac{1}{1 + (b^2 - 1)\beta} \int_\tau^\infty S_{p0}(\eta)\, d\eta, \quad \text{(A 10)}$$

$$B_{pn}(\tau) - B_{pn}(0) \exp(-\mu_n^2 \tau) = \int_0^\tau S_{pn}(\eta) \exp(-\mu_n^2 (\tau - \eta))\, d\eta, \quad \text{(A 11)}$$

with

$$S_{p0}(\tau) = 2p \int_0^1 y W(y) G_1^{(p-1)}\, dy + \frac{p(p-1)}{Pe^2} (m_1^{(p-2)}(\tau) - m_{1\infty}^{(p-2)}(\tau)) + \frac{\lambda p(p-1)}{Pe^2} (b^2 - 1)(m_2^{(p-2)}(\tau) - m_{2\infty}^{(p-2)}\, \tau)), \quad \text{(A 12)}$$

$$S_{pn}(\tau) = \frac{1}{I_{nn}} \left(\int_0^1 y J_0(\mu_n y) \left(p W(y) G_1^{(p-1)} + \frac{p(p-1)}{Pe^2} G_1^{(p-2)} \right) dy + \frac{\lambda p(p-1)}{Pe^2} \int_1^b y M_0(\bar{\mu}_n y) G_2^{(p-2)}\, dy \right). \quad \text{(A 13)}$$

Setting $\tau = 0$ in (A 8) and (A 9), and again applying the orthogonality conditions, yields

$$B_{pn}(0) = \frac{1}{I_{nn}} \left(\int_0^1 y J_0(\mu_n y) C_1^{(p)}(y, 0)\, dy + \int_1^b y M_0(\bar{\mu}_n y) C_2^{(p)}(y, 0)\, dy - N_{pn} \right), \quad \text{(A 14)}$$

where

$$N_{pn} = \int_0^1 y J_0(\mu_n y) C_{1\infty}^{(p)}(y, 0)\, dy + \int_1^b y M_0(\bar{\mu}_n y) C_{2\infty}^{(p)}(y, 0)\, dy, \quad \text{(A 15)}$$

$$B_{p0}(0) = \frac{1}{1 + (b^2 - 1)\beta} (m_1^{(p)}(0) - m_{1\infty}^{(p)}(0) + (b^2 - 1)(m_2^{(p)}(0) - m_{2\infty}^{(p)}(0))). \quad \text{(A 16)}$$

Equating $B_{p0}(0)$ in (A 10) and (A 16) gives

$$m_{1\infty}^{(p)}(0)+(b^2-1)\,m_{2\infty}^{(p)}(0)=m_1^{(p)}(0)+(b^2-1)\,m_2^{(p)}(0)+\int_0^\infty S_{p0}(\eta)\,d\eta. \quad \text{(A 17)}$$

Equation (A 17) is the extra condition required to resolve the undetermined constants in the $C_{i\infty}^{(p)}$ and $m_{i\infty}^{(p)}$. Steady-state results are given in appendix B.

The moments defined by (7) are obtained by taking radial averages of the function $G_i^{(p)}$ to give

$$m_1^{(0)}=m_{1\infty}^{(0)}+2\sum_{n=1}^{\infty}A_n\exp(-\mu_n^2\tau)\frac{J_1(\mu_n)}{\mu_n}, \quad \text{(A 18)}$$

$$m_2^{(0)}=m_{2\infty}^{(0)}-\frac{2}{b^2-1}\sum_{n=1}^{\infty}A_n\exp(-\mu_n^2\tau)\frac{J_1(\mu_n)}{\mu_n}, \quad \text{(A 19)}$$

$$m_1^{(p)}(p\geqslant 1)=m_{1\infty}^{(p)}+B_{p0}(\tau)+2\sum_{n=1}^{\infty}B_{pn}(\tau)\frac{J_1(\mu_n)}{\mu_n}, \quad \text{(A 20)}$$

$$m_2^{(p)}(p\geqslant 1)=m_{2\infty}^{(p)}+\beta B_{p0}(\tau)-\frac{2}{b^2-1}\sum_{n=1}^{\infty}B_{pn}(\tau)\frac{J_1(\mu_n)}{\mu_n} \quad \text{(A 21)}$$

using (A 6).

Pulse-injection case

When $C_1(y, X, 0)=\delta(X)$, $C_2(y, X, 0)=0$ and $W=1-y^2$ (Poiseuille flow), a consideration of (A 7), (A 10)–(A 14) gives

$$A_m=\frac{J_1(\mu_m)}{I_{mm}\mu_m},$$

$$B_{10}(\tau)=-\frac{2}{1+(b^2-1)\beta}\sum_{m=1}^{\infty}\frac{A_m T_m}{\mu_m^2}\exp(-\mu_m^2\tau),$$

$$\underset{n\geqslant 1}{B_{1n}(\tau)}=\frac{1}{I_{nn}}\Big((-N_{1n}+A_n R_{nn}\tau)\exp(-\mu_n^2\tau)-\sum_{\substack{m=1\\ m\neq n}}^{\infty}A_m R_{mn}\Delta_{mn}(\tau)\Big),$$

$$B_{20}(\tau)=-\frac{1}{1+(b^2-1)\beta}\Big(H_{00}(\infty)-H_{00}(\tau)+4\sum_{s=1}^{\infty}T_s(H_{0s}(\infty)-H_{0s}(\tau)),$$

$$+\frac{4}{Pe^2}(1-\lambda)\sum_{s=1}^{\infty}A_s\frac{J_1(\mu_s)}{\mu_s^3}\exp(-\mu_s^2\tau)\Big),$$

$$\underset{n\geqslant 1}{B_{2n}(\tau)}=\frac{1}{I_{nn}}\Big(\Big(-N_{2n}+2(\lambda I_{nn}+(1-\lambda)\,W_{nn})\frac{A_n\tau}{Pe^2}\Big)\exp(-\mu_n^2\tau)$$

$$-\frac{2}{Pe^2}(1-\lambda)\sum_{\substack{s=1\\ s\neq n}}^{\infty}A_s W_{ns}\Delta_{ns}(\tau)+2T_n H_{n0}(\tau)+2\sum_{s=1}^{\infty}R_{ns}H_{ns}(\tau)\Big);$$

where

$$T_n = \int_0^1 y(1-y^2)\,J_0(\mu_n y)\,dy,$$

$$R_{mn} = \int_0^1 y(1-y^2)\,J_0(\mu_m y)\,J_0(\mu_n y)\,dy,$$

$$\Delta_{mn}(\tau) = \frac{\exp(-\mu_m^2\tau)-\exp(-\mu_n^2\tau)}{\mu_m^2-\mu_n^2},$$

$$W_{ns} = \int_0^1 y J_0(\mu_n y)\,J_0(\mu_s y)\,dy,$$

$$H_{ns}(\tau) = \int_0^\tau \exp(-\mu_n^2(\tau-\eta))\,B_{1s}(\eta)\,d\eta \quad (n,s \geqslant 0, \quad \text{taking} \quad \mu_0 = 0).$$

The integrals T_n, R_{mn}, W_{ns}, $H_{ns}(\tau)$ are evaluated as follows:

$$W_{ns} = \frac{\mu_n J_0(\mu_s)J_1(\mu_n)-\mu_s J_0(\mu_n)J_1(\mu_s)}{\mu_n^2-\mu_s^2} \quad (n \neq s),$$

$$= \tfrac{1}{2}(J_0^2(\mu_n)+J_1^2(\mu_n)) \quad (n = s).$$

$$H_{00}(\tau)-H_{00}(\infty) = \frac{2}{1+(b^2-1)\beta}\sum_{m=1}^{\infty}\frac{A_m T_m}{\mu_m^4}\exp(-\mu_m^2\tau),$$

$$H_{0s}(\tau)-H_{0s}(\infty) = \frac{-1}{I_{ss}}\left(\frac{A_s R_{ss}-ET_s}{\mu_s^4}+\frac{A_s R_{ss}\tau}{\mu_s^2}\right)\exp(-\mu_s^2\tau)$$

$$+\frac{1}{I_{ss}}\sum_{\substack{m=1\\ m\neq s}}^{\infty}\frac{A_m R_{sm}}{\mu_m^2-\mu_s^2}\left(\frac{\exp(-\mu_m^2\tau)}{\mu_m^2}-\frac{\exp(-\mu_s^2\tau)}{\mu_s^2}\right) \quad (s \neq 0),$$

$$H_{n0}(\tau) = \frac{-2}{1+(b^2-1)\beta}\left(\frac{A_n T_n}{\mu_n^2}\tau\exp(-\mu_n^2\tau)-\sum_{\substack{m=1\\ m\neq n}}^{\infty}\frac{A_m T_m}{\mu_m^2}\Delta_{mn}(\tau)\right) \quad (n \neq 0),$$

$$H_{nn}(\tau) = \frac{-1}{I_{nn}}\left(\frac{ET_n}{\mu_n^2}-\sum_{\substack{m=1\\ m\neq n}}^{\infty}\frac{A_m R_{mn}}{\mu_m^2-\mu_n^2}-\tfrac{1}{2}A_n R_{nn}\tau\right)\tau\exp(-\mu_n^2\tau)$$

$$+\frac{1}{I_{nm}}\sum_{\substack{m=1\\ m\neq n}}^{\infty}\frac{A_m R_{mn}}{\mu_m^2-\mu_n^2}\Delta_{mn}(\tau) \quad (n \neq 0),$$

$$H_{ns}(\tau) = \frac{-1}{I_{ss}}\left(-\frac{ET_s}{\mu_s^2}+\sum_{\substack{m=1\\ m\neq s}}^{\infty}\frac{A_m R_{ms}}{\mu_m^2-\mu_s^2}-\frac{A_s R_{ss}}{\mu_n^2-\mu_s^2}\right)\Delta_{ns}(\tau)$$

$$+\frac{1}{I_{ss}}\left(\sum_{\substack{m=1\\ m\neq n,s}}^{\infty}\frac{A_m R_{ms}}{\mu_m^2-\mu_s^2}\Delta_{mn}(\tau)-\frac{A_n R_{ns}}{\mu_n^2-\mu_s^2}\tau\exp(-\mu_n^2\tau)\right.$$

$$\left.+\frac{A_s R_{ss}}{\mu_n^2-\mu_s^2}\tau\exp(-\mu_s^2\tau)\right) \quad (n \neq s \neq 0),$$

where the constant E is defined in appendix B.

$$T_n = 2J_2(\mu_n)/\mu_n^2,$$

$$R_{mn} = \frac{2(\mu_m^2+\mu_n^2)(2W_{mn}-J_0(\mu_n)J_0(\mu_m))-4\mu_m\mu_n J_1(\mu_m)J_1(\mu_n)}{(\mu_m^2-\mu_n^2)^2} \quad (m \neq n),$$

$$= \tfrac{1}{4}J_0^2(\mu_n)+\tfrac{1}{3}J_1^2(\mu_n)+\tfrac{1}{12}J_2^2(\mu_n) \quad (m = n),$$

using Watson (1962, p. 136).

Appendix B. Steady-state results

In the treatment by Aris (1959) a single set of moments are defined to include solute in both the tube and the annulus. In this paper the determination of moments defined over the tube alone requires steady-state results, some of which were not needed by Aris. These are presented below.

Under steady-state conditions the centre of mass of solute in both the tube and the annulus moves with the same constant velocity (dimensionless speed $V = \overline{W}/(1+(b^2-1)\beta)$, where $\overline{W}$ is the mean of the velocity profile $W(y)$). Following Aris, we choose an origin moving with speed V and define moments $\nu_{i\infty}^{(p)}(\tau)$ and $\theta_{i\infty}^{(p)}(y,\tau)$ about that point, where

$$\theta_{i\infty}^{(p)}(y,\tau) = \int_{-\infty}^{\infty} (X-V\tau)^p C_i(y,X,\tau)\,dX \quad \text{for large } \tau,$$

$\nu_{i\infty}^{(p)}$ are related to $\theta_{i\infty}^{(p)}$ by (7), and the governing equations can be obtained from (3). The steady-state moments $m_{i\infty}^{(p)}$ defined for a fixed origin can be expressed in terms of those $\nu_{i\infty}^{(p)}$ defined for a moving origin as

$$m_{i\infty}^{(0)} = \nu_{i\infty}^{(0)},$$

$$m_{i\infty}^{(1)} = \nu_{i\infty}^{(1)} + V\tau\nu_{i\infty}^{(0)},$$

$$m_{i\infty}^{(2)} = \nu_{i\infty}^{(2)} + 2V\tau\nu_{i\infty}^{(1)} + V^2\tau^2\nu_{i\infty}^{(0)}$$

for $p = 0, 1, 2$.

When $p = 0$

$$\theta_{1\infty}^{(0)} = \frac{m_1^{(0)}(0)+(b^2-1)\,m_2^{(0)}(0)}{1+(b^2-1)\,\beta} = E,$$

say, is a constant and $\theta_{2\infty}^{(0)} = \beta\theta_{1\infty}^{(0)}$.

When $p = 1$ the $\theta_{i\infty}^{(1)}$ are independent of τ and equivalent to the functions defined by the Aris equations (14) and (15). In particular, we can show, with the aid of (A 17), that

$$\theta_{1\infty}^{(1)} = Ef(y)+\nu_{1\infty}^{(1)}, \tag{B 1}$$

$$\theta_{2\infty}^{(1)} = \beta Eg(y)+\nu_{2\infty}^{(1)}, \tag{B 2}$$

where

$$f(y) = \tfrac{1}{4}V(y^2-\tfrac{1}{2})+\int_y^1 \frac{1}{s}\int_0^s \eta W(\eta)\,d\eta\,ds-\frac{1}{2}\int_0^1 y(1-y^2)\,W(y)\,dy, \tag{B 3}$$

$$g(y) = \frac{V}{2\lambda}\left(\tfrac{1}{2}y^2-b^2\log y+\frac{b^4\log b}{b^2-1}-\tfrac{1}{4}(3b^2+1)\right), \tag{B 4}$$

$$\nu_{1\infty}^{(1)} = \frac{1}{1+(b^2-1)\,\beta}\left(m_1^{(1)}(0)+(b^2-1)\,m_2^{(1)}(0)+\int_0^\infty S_{10}(\eta)\,d\eta+(b^2-1)\,\beta E(g(1)-f(1)\right), \tag{B 5}$$

$$\nu_{2\infty}^{(1)} = \beta\nu_{1\infty}^{(1)}-\beta E(g(1)-f(1)). \tag{B 6}$$

When $p = 2$ it is easy to show that the standard deviation of the solute distribution in the tube changes at the same constant rate K as that in the annulus. That is

$$\frac{d}{d\tau}\left(\frac{\nu_{1\infty}^{(2)}}{\nu_{1\infty}^{(0)}}\right) = \frac{d}{d\tau}\left(\frac{\nu_{2\infty}^{(2)}}{\nu_{2\infty}^{(0)}}\right) = K. \tag{B 7}$$

Since $\nu_{1\infty}^{(0)}$ and $\nu_{2\infty}^{(0)}$ are constants, we also have

$$K = \frac{d}{d\tau}\left(\frac{\nu_{1\infty}^{(2)} + (b^2-1)\,\nu_{2\infty}^{(2)}}{\nu_{1\infty}^{(0)} + (b^2-1)\,\nu_{2\infty}^{(0)}}\right), \tag{B 8}$$

and results corresponding to those derived by Aris for the overall standard deviation apply.

We can show that

$$\tfrac{1}{2}K = \frac{1}{1+(b^2-1)\beta}\left(\frac{1}{Pe^2}(1+\lambda(b^2-1)\beta) + 2\int_0^1 yW(y)f(y)\,dy + (b^2-1)\beta V(g(1)-f(1))\right), \tag{B 9}$$

$$\nu_{1\infty}^{(2)}(0) = \frac{1}{1+(b^2-1)\beta}\left\{m_1^{(2)}(0) + (b^2-1)\,m_2^{(2)}(0) + \int_0^\infty S_{20}(\eta)\,d\eta \right.$$
$$\left. + 2(b^2-1)\,(\nu_{2\infty}^{(1)}\,g(1) - \beta\nu_{1\infty}^{(1)}f(1)) + (b^2-1)\,\beta E L_1 + L_2\right\}, \tag{B 10}$$

where

$$L_1 = -\frac{1}{4}\left(\tfrac{1}{2}K - \frac{1}{Pe^2}\right) + \int_0^1 y(1-y^2)\,W(y)f(y)\,dy + V\int_0^1 y^3 f(y)\,dy, \tag{B 11}$$

$$L_2 = \beta(b^2-1)\frac{E}{\lambda}\left(\tfrac{1}{2}K - \frac{\lambda}{Pe^2}\right)\left(\frac{b^4\log b}{b^2-1} - \tfrac{1}{4}(3b^2-1)\right)$$
$$- \frac{2V\beta E}{\lambda}\left(b^2\int_1^b \frac{1}{y}\int_1^y \eta g(\eta)\,d\eta\,dy + \frac{1}{2}\int_1^b y^3 g(y)\,dy\right). \tag{B 12}$$

For the parabolic flow profile $W = 1-y^2$, (B 9) becomes

$$\tfrac{1}{2}K = R\left(\frac{1}{Pe^2} + \frac{11-16R+6R^2}{192}\right) + (1-R)\left(\frac{\lambda}{Pe^2} + \frac{R^2}{8\lambda}\left(\frac{b^4\log b}{b^2-1} - \tfrac{1}{4}(3b^2-1)\right)\right), \tag{B 13}$$

which may be obtained from the Aris equations (17), (21) and (22), where $R = 1/(1+(b^2-1)\beta)$.

Multiplying the differential equation for $\theta_{1\infty}^{(1)}$ by $yJ_0(\mu_n y)$ and that for $\theta_{2\infty}^{(1)}$ by $yM_0(\mu_n y)$, and adding the two equations, yields an expression for N_{1n} (defined by (A 15)) when the orthogonality conditions (A 5) and (A 6) are applied. Hence

$$N_{1n} = \frac{E}{\mu_n^2}\int_0^1 yJ_0(\mu_n y)\,W(y)\,dy. \tag{B 14}$$

When $p = 2$ the $\theta_{i\infty}^{(2)}$ are linear in τ, and the same treatment of the differential equations for $\theta_{i\infty}^{(2)}(y,0)$ gives

$$N_{2n} = \frac{2}{\mu_n^2}\left(\int_0^1 yJ_0(\mu_n y)\,W(y)\,\theta_{1\infty}^{(1)}\,dy - VN_{1n} + \frac{(1-\lambda)}{Pe^2}E\frac{J_1(\mu_n)}{\mu_n}\right). \tag{B 15}$$

REFERENCES

AHARONSON, E. F., MENKES, H., GURTNER, G., SWIFT, D. L. & PROCTOR, D. F. 1974 Effect of respiratory airflow rate on removal of soluble vapours by the nose. *J. Appl. Physiol.* **37**, 654–657.

ARIS, R. 1959 On the dispersion of a solute by diffusion, convection and exchange between phases. *Proc. R. Soc. Lond.* **A252**, 538–550.

DAVIS, J., KLINOWSKI, J. & WINLOVE, C. P. 1981 Transport of radioactive oxygen, nitrogen and xenon into the rabbit thoracic aorta *in situ*. *Cardiovascular Res.* **15**, 456–461.

DUBOIS, A. B. & ROGERS, R. M. 1968 Respiratory factors determining the tissue concentrations of inhaled toxic substances. *Resp. Physiol.* **5**, 34–52.

GILL, W. N. & SANKARASUBRAMANIAN, R. 1970 Exact analysis of unsteady convective diffusion. *Proc. R. Soc. Lond.* **A316**, 341–350.

HORSFIELD, K. & CUMMING, G. 1968 Morphology of the bronchial tree in man. *J. Appl. Physiol.* **24**, 373–383.

ICHIOKA, M. 1972 Model experiments on absorbability of the airway mucous membrane of SO_2 and NO_2 gases. *Bull. Tokyo Med. Dent. Univ.* **19**, 361–375.

KIRK, J. E. & LAURSEN, T. J. S. 1955 Diffusion coefficients for various solutes for human aortic tissue. With special reference to variation in tissue permeability with age. *J. Gerentol.* **10**, 288–302.

MILLER, F. J., MENZEL, D. B. & COFFIN, D. L. 1978 Similarity between Man and laboratory animals in regional pulmonary deposition of ozone. *Environ. Res.* **17**, 84–101.

LITTLEWOOD, A. B. 1970 *Gas Chromatography. Principles, Techniques and Applications*, p. 141. Academic.

PEARSON, D. A., LUNDBERG, L. A., WEST, F. B. & MCCARTHY, J. L. 1951 Absorption of sulphur dioxide in water in a packed tower. *Chem. Engng Prog.* **47**, 257–264.

PEDLEY, T. J., SCHROTER, R. C. & SUDLOW, M. F. 1977 Gas flow and mixing in the airways. In *Bioengineering Aspects of the Lung* (ed. J. West), pp. 163–265. Dekker.

SCHERER, P. W., SHENDALMAN, L. H., GRENNE, N. M. & BOUHUYS, A. 1975 Measurement of axial diffusivities in a model of the bronchial airways. *J. Appl. Physiol.* **38**, 719–723.

TAYLOR, G. I. 1953 Dispersion of soluble matter in solvent flowing slowly through a tube. *Proc. R. Soc. Lond.* **A219**, 186–203.

ULTMAN, J. S. & BLATMAN, H. S. 1977*a* A compartmental dispersion model for the analysis of mixing in tube networks. *A.I.Ch.E. J.* **23**, 169–176.

ULTMAN, J. S. & BLATMAN, H. S. 1977*b* Longitudinal mixing in pulmonary airways. Analysis of inert gas dispersion in symmetric tube networks. *Resp. Physiol.* **30**, 349–367.

HAYEK, H. VON 1953 *Die menschliche Lunge*. Springer.

WATSON, G. N. 1962 *The Theory of Bessel Functions*, 2nd edn, p. 136. Cambridge University Press.

WEIBEL, E. R. 1963 *Morphometry of the Human Lung*. Academic.

WENDEL, M. M. & PIGFORD, R. L. 1958 Kinetics of nitrogen tetroxide absorption in water. *A.I.Ch.E. J.* **4**, 249–256.

YOKOYAMA, E. 1968 Uptake of SO_2 and NO_2 by the isolated upper airways. *Bull. Inst. Publ. Health* **17**, 302–306.